Available online at www.sciencedirect.com

ScienceDirect

journal homepage: www.elsevier.com/locate/bbe

Original Research Article

Novel expert system for glaucoma identification using non-parametric spatial envelope energy spectrum with fundus images

U. Raghavendra [a,*], Sulatha V. Bhandary [b], Anjan Gudigar [a], U. Rajendra Acharya [c,d,e]

[a] Department of Instrumentation and Control Engineering, Manipal Institute of Technology, Manipal University, Manipal India

[b] Department of Ophthalmology, Kasturba Medical College, Manipal University, Manipal India

[c] Department of Electronics and Computer Engineering, Ngee Ann Polytechnic, Singapore

[d] Department of Biomedical Engineering, School of Science and Technology, Singapore University of Social Sciences, Singapore

[e] Department of Biomedical Engineering, Faculty of Engineering, University of Malaya, Kuala Lumpur Malaysia

ARTICLE INFO

Article history:
Received 30 August 2017
Received in revised form
20 November 2017
Accepted 22 November 2017
Available online 29 November 2017

Keywords:
Computer aided diagnosis
GIST
Glaucoma
Support vector machine
Radon transform

ABSTRACT

Glaucoma is the prime cause of blindness and early detection of it may prevent patients from vision loss. An expert system plays a vital role in glaucoma screening, which assist the ophthalmologists to make accurate decision. This paper proposes a novel technique for glaucoma detection using optic disk localization and non-parametric GIST descriptor. The method proposes a novel area based optic disk segmentation followed by the Radon transformation (RT). The change in the illumination levels of Radon transformed image are compensated using modified census transformation (MCT). The MCT images are then subjected to GIST descriptor to extract the spatial envelope energy spectrum. The obtained dimension of the GIST descriptor is reduced using locality sensitive discriminant analysis (LSDA) followed by various feature selection and ranking schemes. The ranked features are used to build an efficient classifier to detect glaucoma. Our system yielded a maximum accuracy (97.00%), sensitivity (97.80%) and specificity (95.80%) using support vector machine (SVM) classifier with *nineteen* features. Developed expert system also achieved maximum accuracy (93.62%), sensitivity (87.50%) and specificity (98.43%) for public dataset using *twenty six* features. The proposed method is efficient and computationally less expensive as it require only *nineteen* features to model a classifier for the huge dataset. Therefore the proposed method can be effectively utilized in hospitals for glaucoma screening.

* *Corresponding author at*: Department of Instrumentation and Control Engineering, Manipal Institute of Technology, Manipal University, Manipal 576104, India.
E-mail address: raghavendra.u@manipal.edu (U. Raghavendra).

https://doi.org/10.1016/j.bbe.2017.11.002

1. Introduction

Glaucoma is one of the eye disorders caused by optic nerve damage leading to partial or complete blindness. It is an irreversible and chronic condition which progressively damage the optic nerve [1,2]. It is estimated that by 2020, there will be approximately 80 million people worldwide affected by glaucoma [3–5].

The nerve fibers can be represented by an annular region between cup boundary and the optic disk (OD) known as neuroretinal rim [3] and the fluid pressure inside the eye is referred to as intraocular pressure (IOP) [6,7]. Thus leading to the blockage of outflow of aqueous humor. This will damage the optic nerve which transmits the information from retina to the brain [4,5]. The loss of optic nerve fibers are probably due to high IOP. The deterioration of optic nerve fibers lead to the decrease in the thickness of retinal nerve fiber layer (RNFL) called cupping which is a significant cause for glaucoma progression [3,8]. An increased cup to disk ratio (CDR) indicates the decrease in the quantity of healthy neuro-retinal tissue and hence displaying a glaucomatous change [8]. The healthy eye usually has a CDR of 0.3 [6,9].

Glaucoma can be broadly classified into the three stages (mild, moderate and severe) depending on the CDR in the fundus image [10,11]. Mild stage indicates the progress of glaucoma hinting the enlargement of the cup and CDR at this stage is usually between 0.4 and 0.5. Moderate will be in the range 0.5–0.7 and severe glaucoma is an advanced stage where the CDR is usually more than 0.7 [11]. In moderate cases, the central vision may not be affected. But if not diagnosed and treated, the severe stage of glaucoma can eventually lead to blindness [11–13].

Digital fundus image analysis is valuable to understand the natural development of the disease which relies on computational techniques to make qualitative assessments of the eye [14–17]. Fundus image is a 2D projection of the retinal structures. The OD is a bright circular or elliptical region partially occluded by blood vessels. In 2D retinal fundus images, OD can be divided into a central bright zone called the optic cup and peripheral region called the neuroretinal rim [18]. In comparison with optical coherence tomography (OCT)/ Heidelberg retina topography (HRT) machines, the fundus camera is economical, easier to operate and is appropriate to estimate various eye conditions [9]. The geometric parameters that measure the changing structures of Optic Nerve Head (ONH) such as the diameter of the OD, area of the OD, cup diameter, area of the rim, and mean cup depth are vital in diagnosing this disorder [14]. The CDR is computed as the ratio of the vertical cup diameter to the vertical disk diameter clinically. A larger CDR generally indicates a higher risk of glaucoma and vice versa. A non-invasive, portable and cost effective glaucoma diagnosis tools are the most essential requirement in primary healthcare centers [19–21].

There are many techniques proposed to calculate CDR which uses segmentation of optic disk and the cup [22–24]. It involves contour based approach [25], fuzzy convergence [26], template based method [27], Hough transform [28] and geometric model based technique [29]. Joshi et al. (2012) [30] have proposed a method to find CDR based on depth discontinuity model with mean CDR error of 0.09. A morphological method is proposed in [31]. Xu et al. (2011) [32] have proposed a method to find CDR which coupled feature extraction with SVM classifier. Thresholding and edge detection based methods are also proposed in [33].

Various CAD techniques are reported in the literature for automated detection as well as classification of normal and glaucoma classes [34–36]. A unique method for glaucoma diagnosis is developed in [37] using higher order spectra (HOS) features and textures. They reported an accuracy of more than 91% using 60 fundus images. Dua et al. (2012) [38] proposed a method which uses energy signatures obtained using 2D discrete wavelet transform (DWT). The experiment was performed on 60 fundus images and achieved an accuracy of 93%. Mookiah et al. (2012) [39] proposed an automated system using HOS and DWT features with 95% accuracy, 93.33% sensitivity and 96.67% specificity. Kim et al. (2011) [40] have used fractal analysis (FA) as the groundwork for multiclass prediction of the progression of glaucoma. The box-counting method is used to obtain monofractal features while the multifractional Brownian motion method is used to obtain multifractal features, thereby incorporating texture and multiresolution analysis. Noronha et al. (2014) [41] developed a new method using HOS cumulants features. They achieved maximum of 92.65% accuracy, 100% sensitivity and 92% specificity. Yousefi et al. (2014) [42] developed a method to detect glaucomatous progression using different machine learning classifiers. The experiment was conducted on 632 images and the AUROC (95% CI) of 0.88 is achieved when selecting 10 best features using random forest tree classifier. Ceccon et al. (2014) [43] developed method based on Bayesian network concurrently to classify early glaucoma and cluster data into different stages of disease. They have achieved a sensitivity of 50% and specificity of 90% for pre diagnosis data whereas 85% sensitivity and 90% specificity for post diagnosis data. Maheshwari et al. (2017) [44] have developed a model using 2D empirical wavelet transform and achieved 98.33% accuracy for 60 images. The same group have extended their work using variational mode decomposition and achieved 95.19% accuracy for 488 fundus images [45]. Recently Acharya et al. (2017) [46] have proposed a method using texton and local configuration patterns. They reported a maximum accuracy of 95.70% using kNN classifier for 702 fundus images.

It can be observed from the literature that the existing techniques for glaucoma screening involve, manual, semi-automated and fully automated diagnosis. Manual and semi-automated methods are tedious and prone to inter and intra observer errors while reading the images. Hence, this paper presents a novel datamining technique for glaucoma screening using non-parametric GIST descriptor. The proposed method initially developed an optic disk (OD) segmentation technique followed by feature representation using Radon transform (RT). The effect of change in illumination and color on Radon transformed image is compensated using modified census transform (MCT). Further, spatial envelope features are computed from non-parametric MCT images and the dimensions of the extracted spatial envelope features are reduced using locality sensitive discriminant analysis (LSDA). Reduced features are selected and ranked using *t-test* based statistical measures.

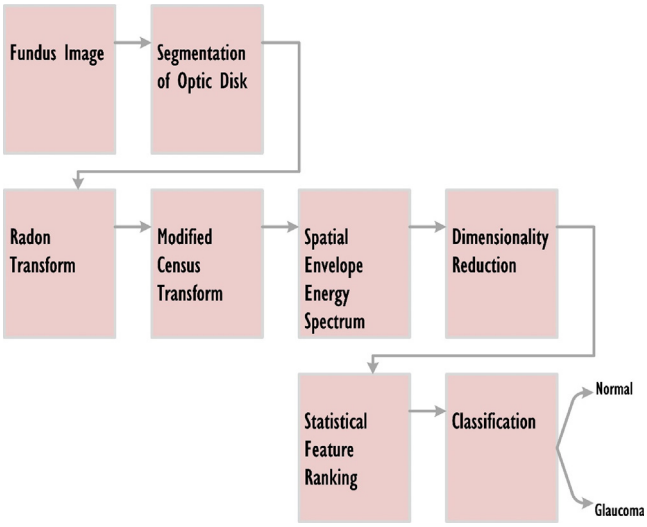

Fig. 1 – Block diagram of the developed model.

Ranked features are subjected to support vector machine (SVM) classifier for the evaluation. The developed method is systematically evaluated using a diverse private and public datasets. Overview of the developed model is given in Fig. 1.

2. Materials and methods

2.1. *Fundus image description*

We have used 1000 fundus images (normal: 500, glaucoma: 500) in this study. The images were taken from Kasturba Medical College and Hospital, Manipal, India. Image were captured using ZEISS fundus camera, which stores acquired images into JPEG image format with a resolution of 2588 × 1958 pixels. Institutional ethical approval has been received prior to the study. Fig. 2 shows sample fundus images. We have also used a public dataset for our evaluation [47]. It included 255 normal and 200 glaucoma fundus images.

2.2. *Optic disk localization*

In general, OD appears to have highest contrast against background in red plane. Therefore, we have used red plane to perform our initial segmentation. The precise segmentation of OD is difficult due to blood vessel inference. Thus, a median filter of size 5 × 5 is applied on red plane to remove the blood vessels and retain the shape of OD. Further, image pixel values are enhanced using similar algorithm proposed in [48].

Then the median filter is applied over the enhanced image and the features such as exudates, cotton wool, spots may interfere the OD segmentation, as it shows brightness pigmentation. Hence, empirically we have selected an adaptive search window to detect OD in the fundus image. The entire retinal image is scanned with this adaptive window and connected component with the larger area is selected as OD. Finally, the selected region is extracted from the retinal image for further processing. Different stages of optic disk segmentation is shown in Fig. 3.

2.3. *Radon transform (RT)*

The Radon function is a projection of intensities along a radial line for a specified angle. The transform is commonly used to represent the projection data and is as such applicable to fundus images [49,50]. Fig. 4 shows the Radon transform of normal and glaucoma image for 0–179° orientations.

2.4. *Non-parametric local transform*

Non-parametric features are the local spatial features which convey the information about the order in which the intensities are distributed within a neighborhood region rather than their original intensity values. Hence, they can compensate illumination variation. Census transform (CT) [51] is one such method frequently experimented in computer vision research. MCT is an extended version of CT, which compares each neighborhood point with the mean intensity of center pixel. Let $\eta'(x)$ be a local neighborhood with center pixel at x.

Fig. 2 – Sample fundus images of normal and glaucoma classes from our private database.

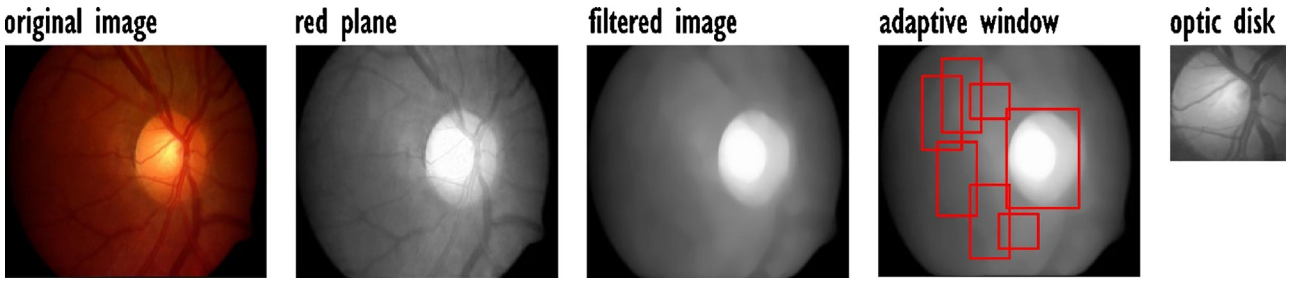

Fig. 3 – Illustration of optic disk segmentation.

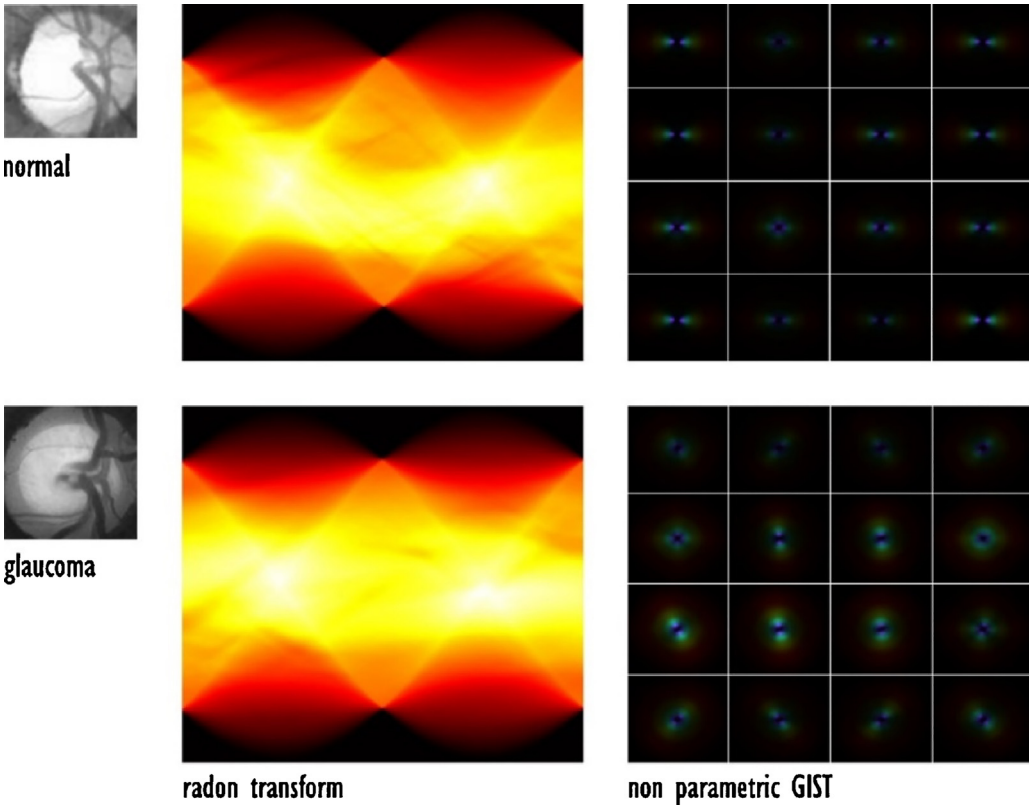

Fig. 4 – Radon and non-parametric GIST of normal and glaucoma images.

The mean intensity of the neighborhood is given by $I'(x)$. Here, the original CT is reformulated as:

$$\tau(x) = \otimes_{y \in \eta'} \zeta(I'(x), I(y)) \quad (1)$$

where $\zeta(\cdot)$ shows a single sensor comparison, $\tau(x)$ is the MCT bit string and $\otimes$ defines concatenation operation. Eq. (1) determines all possible kernel structure (512) defined by the local neighborhood. Hence, it effectively captures any different local image structure caused by the local illumination variations [52]. In this work, radon transferred fundus images are subjected to MCT for compensating change in illumination and color.

2.5. *Feature extraction using GIST descriptors*

Image shape places a key role in feature extraction in majority of medical image analysis [53]. The method need to efficiently represent the suspicious abnormality using a particular mathematical model. The GIST is a type of descriptor, which represent the image in terms of its local structure [53]. Initially, gray-scale glaucomatous images are convolved by means of Gabor filters with different orientations and scales. The resultant feature map is subdivided into sixteen regions and the averaged values of feature within each region of interest are calculated. Finally all the features are concatenated to describe the feature of normal and glaucomatous image. In this work, *thirty-two* Gabor filters with 4 scales and 8 orientations are used to generate 32 feature maps with 512 features. The GIST produces the low dimensional feature vector by providing gradient information [53–55,61]. Fig. 4 shows the extracted non-parametric GIST from normal and glaucoma images, as it is extracted from the MCT images.

2.6. *Dimensionality reduction*

Generally, digital image analysis techniques produce high dimensional data [55–63]. This demands dimensionality reduction technique for the real-time processing. Hence, in this work we have used an efficient data reduction method called locality sensitive discriminant analysis (LSDA). A fundamental descriptions of LSDA is presented in [64]. It is a supervised dimensionality reduction method, which preserves both local structure and discrimination among different data points using within-class graph and the between-class graph. In order to get the optimal solution a specific objective function is solved to maximize the distance between inter class data samples.

2.7. *Feature selection*

Majority of spatial features exhibit irrelevant and trivial data samples. Feature selection helps to improve the performance, brings cost effective and faster models [65]. Receiver operating characteristic (roc) [66], Student's *t*-test [67], entropy [68,69], Wilcoxon rank tests [70–73] and Bhattacharyya distance [74], are the commonly used ranking methods used for feature selection.

3. Classification

Classifiers are the predictive models, which identify the class of a test dataset using supervised and unsupervised techniques. In this work, we have used an efficient support vector machine classifier (SVM) [75] for the evaluation of proposed model. The major significant attribute of SVM classifier is its kernel function and the hyper plane, where it aims at making a decision boundary [75,76]. In case, if features are not possible to separate linearly, non-linear kernels namely radial basis function (RBF) and polynomials of order 1, 2 and 3 kernels are used.

4. Results

The proposed methodology is evaluated using 1000 fundus images (500 normal and 500 glaucoma). Initially, normal and glaucoma images are subjected to RT followed by MCT to compensate the change due to illumination [51]. Then, we have extracted 512 GIST features from normal and glaucoma images as shown in Fig. 4. The LSDA is used for data dimensionality reduction, which resulted in *thirty* most significant features. A set of feature ranking methods are used to select the best differentiable features from *thirty* significant features. Finally, an efficient classification model is developed using ten-fold cross validation strategy. The proposed method is evaluated using sensitivity, specificity, accuracy and positive predictive value (PPV). The following section presents the details of the results obtained.

Table A1 presents the *mean* and standard deviation of *t*-test ranked features as it gives maximum performance compared to other ranking techniques. It can be seen from Table 1 that, *t-test* based ranking achieved maximum performance for private dataset with SVM classifier. We have obtained the highest performance of 97.8% sensitivity, 95.8% specificity, 97% accuracy and 95.88% PPV using *nineteen* features. Fig. 5 shows the performance measures obtained using *t*-test based ranking with SVM classifier for private dataset. Fig. 6 shows the accuracy (%) for various kernel functions of SVM classifier versus different ranking methods. It can be noted that *poly 2* has performed better among different ranking techniques and kernel functions. Table 2 shows the best performance achieved using different ranking methods for public dataset. Fig. 7 shows the performance measures obtained using Wilcoxon ranking method for public dataset with SVM classifier. Fig. 8 presents the variation of accuracy (%) for various kernel functions of SVM classifier with respect to different ranking methods using public dataset. It can be observed that *poly 1* has performed better for public dataset. Fig. 9 shows that after performing LSDA, the features separate clearly between the two (normal and glaucoma) classes using graph embedding technique yielding highest classification performance. In order to generalize our method, we have performed experiments using different classifiers such as decision tree (DT) [86,87], linear discriminant analysis (LDA), quadratic discriminant analysis (QDA) [88–90] and fuzzy sugeno classifier [91]. Obtained results are presented in Tables 3 and 4.

5. Discussion

This work developed a non-parametric GIST descriptor for the detection of glaucoma risk. Initially we have extracted a non-parametric GIST features from all radon transformed images, which gives two distinct features for normal and glaucoma as shown in Fig. 4. The extracted features are subjected to LSDA based graph embedding which has enhanced the overall discrimination power of the proposed method among two classes. Various CAD techniques on glaucoma detection is presented in the literature and are listed in Table 5. In addition, many researchers have detected the OD location using different methods [27,77,78]. In our proposed segmentation, the median filter is used to eliminate the influence of blood vessels. We have analyzed OD as one of the largest blob in the binary image during segmentation. The adaptive window is generated to fix the size of OD location. Once OD is fixed, the region of interest is extracted from the original fundus image. The RT is applied to capture the minute changes. Also MCT is applied to efficiently compensate the influence of changes in the illumination on the Radon transformed image.

The GIST is performed on the MCT image and it accumulates the information over the sub region of OD and these features are invariant to illumination, contrast, etc. The LSDA brings the discrimination in the features by constructing graph, based on inter and intra-class weight matrix as shown in Fig. 9. Also, it brings an optimal solution by maximization to separate the normal and glaucoma effectively. Further, these features are categorized using SVM, as it is less susceptible to over fit [75,76]. We have achieved promising accuracy for both private and public datasets. It can be observed that using poly 2 kernel, sensitivity of the system is approximately 98% and specificity is approximately 96% for the private dataset. The obtained false positive and false negative cases are 21 and 11 respectively using only *nineteen* features. It is observed

Table 1 – Best performance for different ranking methods with private dataset.

Ranking	Kernel	NOF	G_{TP}	G_{TN}	G_{FP}	G_{FN}	G_{acc} (%)	G_{PPV} (%)	G_{SEN} (%)	G_{SPE} (%)
Bhattacharya	Poly 2	25	483	476	24	17	95.90	95.26	96.60	95.20
Entropy	Poly 2	25	483	476	24	17	95.90	95.26	96.60	95.20
Roc	RBF	14	490	475	25	10	96.50	95.14	98.00	95.00
t-test	Poly 2	19	489	479	21	11	97.00	95.88	97.80	95.80
Wilcoxon	RBF	12	475	488	12	25	96.30	97.53	95.00	97.60

* G_{TP}: true positive, G_{TN}: true negative, G_{FP}: false positive, G_{FN}: false negative, NOF: number of features, G_{acc}: accuracy, G_{PPV}: positive predictive value, G_{SEN}: sensitivity, G_{SPE}: specificity.

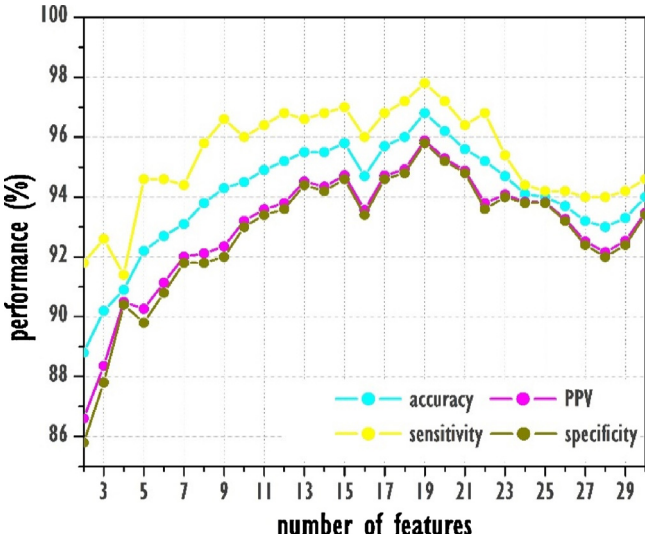

Fig. 5 – Different performance measures for t-test ranking method using private dataset with SVM classifier.

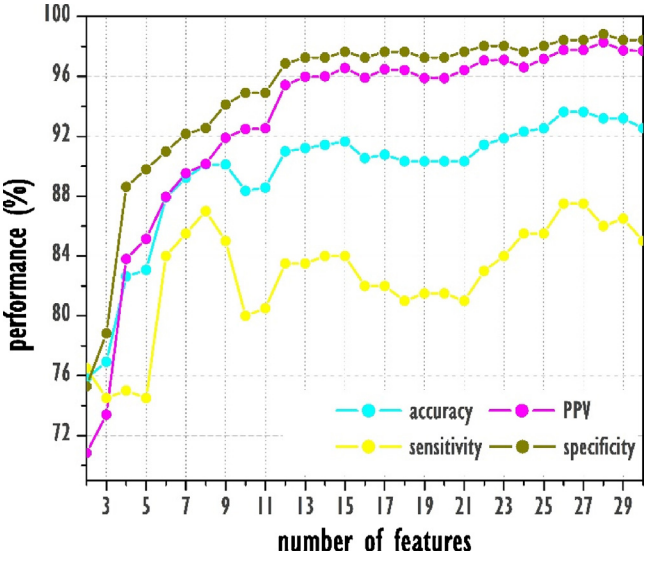

Fig. 7 – Different performance metrics for Wilcoxon ranking method using public dataset.

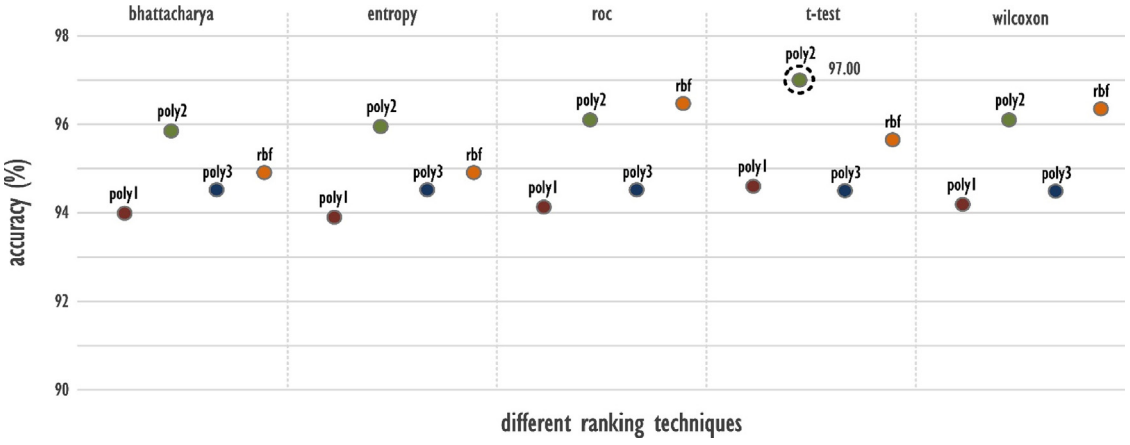

Fig. 6 – Variation of accuracy (%) for various kernel functions of SVM classifier versus different ranking methods with private dataset.

Table 2 – Best performance for different ranking methods with public dataset.

Ranking	Kernel	NOF	G_{TP}	G_{TN}	G_{FP}	G_{FN}	G_{acc} (%)	G_{PPV} (%)	G_{SEN} (%)	G_{SPE} (%)
Bhattacharya	Poly 1	28	172	250	5	28	92.74	97.17	86.00	98.03
Entropy	Poly 1	28	172	250	5	28	92.74	97.17	86.00	98.03
Roc	Poly 2	11	179	244	11	21	92.96	94.21	89.50	95.68
t-test	Poly 1	23	170	252	3	30	92.74	98.26	85.00	98.82
Wilcoxon	Poly 1	26	175	251	4	25	93.62	97.76	87.50	98.43

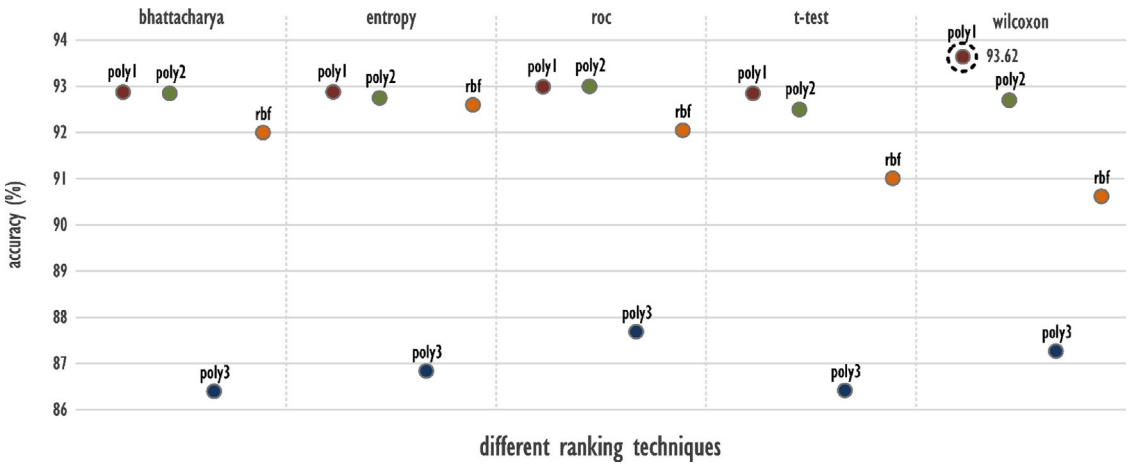

Fig. 8 – Variation of accuracy (%) for various kernel functions of SVM classifier versus different ranking methods with public dataset.

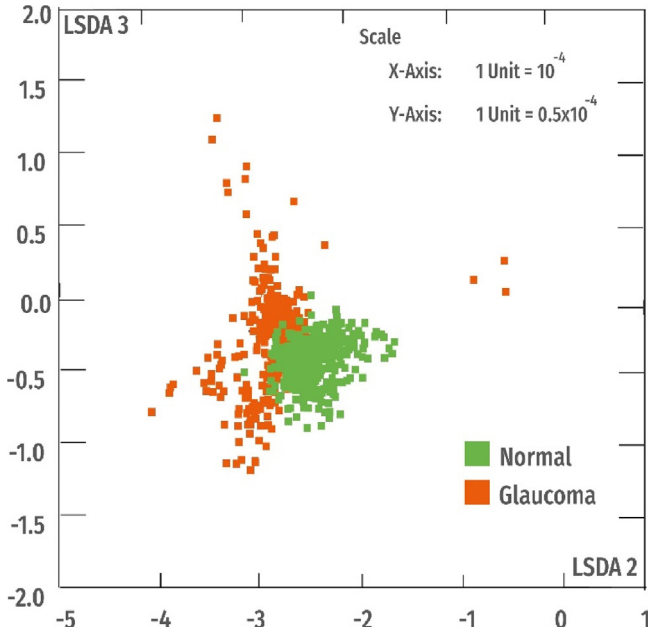

Fig. 9 – Scatter plot showing separation between normal and glaucoma features after LSDA.

Table 3 – Best performance obtained with different classifiers for private dataset.

Classifiers	NOF	G_{TP}	G_{TN}	G_{FP}	G_{FN}	G_{acc} (%)	G_{PPV} (%)	G_{SEN} (%)	G_{SPE} (%)
DT	5	457	461	39	43	91.80	92.13	91.40	92.20
LDA	18	455	464	36	45	91.90	92.66	91.00	92.80
QDA	3	459	406	94	41	86.50	83.00	91.80	81.20
Fuzzy	7	458	478	22	42	93.60	95.41	91.60	95.60

Table 4 – Best performance obtained with different classifiers for public dataset.

Classifiers	NOF	G_{TP}	G_{TN}	G_{FP}	G_{FN}	G_{acc} (%)	G_{PPV} (%)	G_{SEN} (%)	G_{SPE} (%)
DT	8	177	231	24	23	89.67	88.05	88.50	90.58
LDA	30	148	250	5	52	87.47	96.73	74.00	98.03
QDA	3	106	238	17	94	75.60	86.17	53.00	93.33
Fuzzy	8	171	248	7	29	92.08	96.06	85.50	97.25

Table 5 – Summary of the works conducted on automated detection of glaucoma.

Author	Features	Images	Classifier	Performance (%)
Townsend et al. [79]	HRT parameters	200	SVM, RPART	G_{acc}: 87.50
Fink et al. [80]	HRT parameters/ICA	120	kNN	G_{acc}: 91.00
Nagarajan et al. [81]	M-VEP		ANN	G_{acc}: 94.50 G_{sen}: 95.00 G_{spe}: 94.00
Bock et al. [82]	PCA, FFT and spline	575	SVM	G_{acc}: 80.00 G_{sen}: 73.00 G_{spe}: 85.00
Huang et al. [83]	RNFL	165	ANN, LDA	AROC: 0.932 G_{sen}: 83.54 G_{spe}: 93.02
Kolar and Jan [84]	Fractal + power spectral features	30	SVM	G_{acc}: 75.00
Acharya et al. [37]	HOS + texture	60	Random Forest	G_{acc}: 91.00
Dua et al. [38]	Wavelet energy	60	SMO	G_{acc}: 93.00
Mookiah et al. [39]	HOS + wavelet	60	SVM	G_{acc}: 95.00 G_{sen}: 93.33 G_{spe}: 96.67
Norohna et al. [41]	HOS cumulants	272	NB	G_{acc}: 92.65 G_{sen}: 100.00 G_{spe}: 92.00
Acharya et al. [85]	Gabor features	510	SVM	G_{acc}: 93.10 G_{sen}: 89.75 G_{spe}: 96.20
Maheshwari et al. [44]	2-D EWT and correntropy	60	SVM	G_{acc}: 98.33 G_{sen}: 96.67 G_{spe}: 100.00
Maheshwari et al. [45]	VMD	488	LS-SVM	G_{acc}: 95.19 G_{sen}: 93.62 G_{spe}: 96.71
Acharya et al. [46]	Texton and LCP	702	kNN	G_{acc}: 95.70 G_{sen}: 96.20 G_{spe}: 93.70
Our method	Radon + MCT + GIST + LSDA	1000	SVM	Private: G_{acc}: 97.00 Public: G_{acc}: 93.62

that proposed method with SVM classifier performs better compared to other classification techniques (Ref. Tables 3 and 4). Also the developed system has very few false negative cases, indicating that maximum number of glaucoma cases are identified correctly. To the best of our knowledge, we have attained the maximum performance using maximum number of fundus images (Ref. Table 5).

Our system is developed using 1000 fundus images. The computation time of 14.31 s for training and 6.56 s for testing with SVM Poly2, for our system configuration of Intel *Corei*5 with 4 GB RAM.

The main advantages of our proposed system are summarized below:

1. Developed a novel optic disk segmentation for the detection of glaucoma.
2. Used highest number (500: normal, 500: glaucoma) of fundus images.
3. Obtained highest performance using only *nineteen* features. Hence, it can be used as customized device in polyclinics and hospitals.
4. The results are robust and reproducible as it established over ten-fold cross validation.

6. Conclusion

Glaucoma is one of the irreversible eye disease which will damage the optic nerve head causing permanent vision loss. Early detection and timely treatment is most essential to save the vision. In this paper, we have developed a novel expert system for the detection of glaucoma using non-parametric GIST descriptor. Developed model used 1000 fundus images and achieved the highest accuracy of 97.00% using private dataset. The obtained performance reveals that the model can predict glaucoma in its early stage as it achieves maximum sensitivity (≈98%) which may help patients to undergo early treatment. Since, the model is evaluated using a huge number of fundus images with ten-fold cross validation, it can be used as customized device to assist ophthalmologists during their routine screening. In future, we intend to develop a deep learning model by including diverse dataset with early, medium and severe glaucoma images. We plan to extend this technique to detect other retinal diseases namely, diabetic retinopathy, maculopathy, retinal detachment and age related macular degeneration, etc.

Appendix A. Appendix

See Table A1.

Table A1 – *Mean* and standard deviation (SD) of *t-test* ranked *nineteen* significant features.

	Normal		Glaucoma		*p*-value	Criterion
	Mean	SD	Mean	SD		
LSDA2	−0.00029	3.18×10^{-5}	−0.00025	2.1×10^{-5}	3.19×10^{-98}	23.602
LSDA3	-2.9×10^{-5}	3.33×10^{-5}	-4.4×10^{-5}	1.4×10^{-5}	1.63×10^{-19}	9.226
LSDA6	3.63×10^{-5}	3.51×10^{-5}	4.97×10^{-5}	1.61×10^{-5}	1.51×10^{-14}	7.803
LSDA1	-7.6×10^{-5}	3.46×10^{-5}	-6.8×10^{-5}	1.12×10^{-5}	4.11×10^{-7}	5.097
LSDA10	-7.6×10^{-5}	4.07×10^{-5}	-8.3×10^{-5}	2.07×10^{-5}	0.0009	3.317
LSDA4	−0.0001	5.56×10^{-5}	−0.00011	2.02×10^{-5}	0.0022	3.060
LSDA12	-1×10^{-5}	3.96×10^{-5}	-4.9×10^{-6}	2.01×10^{-5}	0.0059	2.756
LSDA9	0.00011	4.22×10^{-5}	0.000104	2.43×10^{-5}	0.0085	2.634
LSDA14	8.24×10^{-5}	2.45×10^{-5}	8.58×10^{-5}	2.73×10^{-5}	0.0374	2.083
LSDA29	−0.00021	3.11×10^{-5}	−0.00021	2.53×10^{-5}	0.0762	1.774
LSDA22	3.99×10^{-5}	2.93×10^{-5}	3.74×10^{-5}	1.55×10^{-5}	0.0877	1.708
LSDA20	-4.3×10^{-5}	2.8×10^{-5}	-4×10^{-5}	1.82×10^{-5}	0.1707	1.370
LSDA25	-1.4×10^{-5}	2.47×10^{-5}	-1.7×10^{-5}	2.82×10^{-5}	0.1879	1.317
LSDA30	7.91×10^{-5}	2.19×10^{-5}	7.74×10^{-5}	2.25×10^{-5}	0.2271	1.208
LSDA28	−0.00026	3.2×10^{-5}	−0.00026	3.03×10^{-5}	0.2461	1.160
LSDA17	6.3×10^{-6}	2.94×10^{-5}	8.7×10^{-6}	3.79×10^{-5}	0.2639	1.117
LSDA27	6.76×10^{-5}	3.3×10^{-5}	6.57×10^{-5}	2.18×10^{-5}	0.2821	1.075
LSDA13	-6.3×10^{-5}	4.32×10^{-5}	-6.5×10^{-5}	2.16×10^{-5}	0.3094	1.016
LSDA19	5.15×10^{-5}	3.06×10^{-5}	5.31×10^{-5}	1.69×10^{-5}	0.3097	1.016

REFERENCES

[1] Lim R, Goldberg I. The glaucoma book: a practical, evidence-based approach to patient care; 2010;3, Chapter 1.

[2] Lim TC, Chattopadhyay S, Acharya UR. A survey and comparative study on the instruments for glaucoma detection. Med Eng Phys 2012;34(2):129–39.

[3] Bourne RRA. The optic nerve head in glaucoma. Commun Eye Health 2006;19(59):44–5.

[4] Sommer A, Tielsch JM, Katz J, Quigley HA, Gottsch JD, Javitt J, Singh K. Relationship between intraocular pressure and primary open angle glaucoma among white and black Americans. The Baltimore Eye Survey. Arch Ophthalmol 1991;109(8):1090–5.

[5] Quigley HA, Broman AT. The number of people with glaucoma worldwide in 2010 and 2020. Br J Ophthalmol 2006;90(3):262–7.

[6] Goldmann H, Schmidt T. Applanation tonometry. Ophthalmologica 1957;134:221–42.

[7] Acharya UR, Ng EYK, Suri JS. Image modeling of the human eye, Artech House bioinformatics & biomedical imaging series. Artech House; 2008.

[8] Burgoyne CF. Pearls of glaucoma management. Berlin, Heidelberg: Springer; 2010. p. 1.

[9] Eye Diseases Prevalence Research Group. Prevalence of open-angle glaucoma among adults in the United States. Arch Ophthalmol 2004;122:532–8.

[10] Nordmann JP, Mesbah M, Berdeaux G. Scoring of visual field measured through Humphrey perimetry: principal component varimax rotation followed by validated cluster analysis. Invest Ophthalmol Vis Sci 2005;46:3169–76.

[11] Sharma P, Sample PA, Zangwill LM, Schuman JS. Diagnostic tools for glaucoma detection and management. Surv Ophthalmol 2008;53(1):S17–32.

[12] Yannuzzi LA, Ober MD, Slakter JS, Spaide RF, Fisher YL, Flower RW, Rosen R. Ophthalmic fundus imaging: today and beyond. Am J Ophthalmol 2004;137(3):511–24.

[13] Acharya UR, Yun WL, Ng EYK, Yu W, Suri JS. Imaging systems of human eye: a review. J Med Syst 2008;32(4):301–315.

[14] Noronha K, Acharya UR, Nayak KP, Kamath S, Bhandary SV. Decision support system for diabetic retinopathy using discrete wavelet transform. Proc Inst Mech Eng Part H J Eng Med 2013;227(3):251–61.

[15] Acharya UR, Chua CK, Ng EYK, Yu W, Chee C. Application of higher order spectra for the identification of diabetes retinopathy stages. J Med Syst 2008;32(6):481–8.

[16] Acharya UR, Lim CM, Ng EYK, Chee C, Tamura T. Computer-based detection of diabetes retinopathy stages using digital fundus images. Proc Inst Mech Eng Part H J Eng Med 2009;223(5):545–53.

[17] Yun WL, Acharya UR, Venkatesh YV, Chee C, Lim CM, Ng EYK. Identification of different stages of diabetic retinopathy using retinal optical images. Int Sci 2008;178(1):106–21.

[18] Chrástek R, Wolf M, Donath K, Niemann H, Paulus D, Hothorn T, Lausen B, Lämmer R, Mardin C, Michelson G. Automated segmentation of the optic nerve head for diagnosis of glaucoma. Med Image Anal 2005;9(4):297–314.

[19] Kanski JJ, McAllister JA, Salmon JF. Glaucoma: a colour manual of diagnosis and treatment. 2nd ed. Oxford; Boston: Butterworth-Heinemann; 1996.

[20] Glaucoma Guide; 2010. Available: http://www.medrounds.org/glaucomaguide/2006/02/section-1-b-meaning-of-cupping.html.

[21] Vingrys AJ. The many faces of glaucomatous optic neuropathy. Clin Exp Optomet 2000;83:145–60.
[22] Betz P, Camps F, Collignon-Brach J, Lavergne G, Weekers R. Biometric study of the disc cup in open-angle glaucoma. Graefes Arch Clin Exp Ophthalmol 1982;218(2):70–4.
[23] Kourkoutas D, Karanasiou IS, Tsekouras GJ, Moshos M, Iliakis E, Georgopoulos G. Glaucoma risk assessment using a non-linear multivariable regression method. Comput Methods Programs Biomed 2012;108(3):31149–5.
[24] Xu J, Chutatape O, Sung E, Zheng C, Kuan PCT. Optic disk feature extraction via modified deformable model technique for glaucoma analysis. Pattern Recognit 2007; 40(7):2063–76.
[25] Xu J, Chutatape O, Chew P. Automated optic disk boundary detection by modified active contour model. IEEE Trans Biomed Eng 2007;54(3):473–82.
[26] Hoover A, Goldbaum M. Locating the optic nerve in a retinal image using the fuzzy convergence of the blood vessels. IEEE Trans Biomed Eng 2003;22(8):951–8.
[27] Lalonde M, Beaulieu M, Gagnon L. Fast and robust optic disc detection using pyramidal decomposition and Hausdorff-based template matching. IEEE Trans Med Imag 2011; 20(11):1193–200.
[28] Fleming AD, Goatman KA, Philip S, Olson JA, Sharp PF. Automatic detection of retinal anatomy to assist diabetic retinopathy screening. Phys Med Biol 2007;52(2):331–45.
[29] Foracchia M, Grisan E, Ruggeri A. Detection of optic disc in retinal images by means of a geometrical model of vessel structure. IEEE Trans Biomed Eng 2004;23(10):1189–95.
[30] Joshi G, Sivaswamy J, Krishnadas SR. Depth discontinuity-based cup segmentation from multiview color retinal images. IEEE Trans Biomed Eng 2012;59(6):1523–31.
[31] Nayak J, Acharya UR, Bhat PS, Shetty A, Lim TC. Automated diagnosis of glaucoma using digital fundus images. J Med Syst 2009;33(5):337–46.
[32] Xu Y, Xu D, Lin S, Liu J, Cheng J, Cheung CY, Aung T, Wong TY. Sliding window and regression based cup detection in digital fundus images for glaucoma diagnosis. Medical Image Computing and Computer-Assisted Intervention – MICCAI 2011, 14. Berlin, Heidelberg: Springer; 2011. p. 1–8.
[33] Yuji H, Noudo A, Muramatsu C, Sawada A, Hara T, Yamamoto T, Fujita H. Vertical cup-to-disc ratio measurement for diagnosis of glaucoma on fundus images. SPIE Medical Imaging. International Society for Optics and Photonics; 2010. p. 76243C.
[34] Balasubramanian M, Zabic S, Bowd C, Thompson HW, Wolenski P, Iyengar SS, Karki BB, Zangwill LM. Clinical evaluation of the proper orthogonal decomposition framework for detecting glaucomatous changes in human subjects. Invest Ophthalmol Vis Sci 2010;51:264–71.
[35] Boquete L, Miguel-Jiménez JM, Ortega S, Rodríguez-Ascariz JM, Pérez-Rico C, Blanco R. Multifocal electroretinogram diagnosis of glaucoma applying neural networks and structural pattern analysis. Expert Syst Appl 2012;39(1): 234–238.
[36] Huang ML, Chen HY, Huang JJ. Glaucoma detection using adaptive neuro-fuzzy inference system. Expert Syst Appl 2007;32(2):458–68.
[37] Acharya UR, Dua S, Du X, Sree SV, Chua CK. Automated diagnosis of glaucoma using texture and higher order spectra features. IEEE Trans Inf Technol Biomed 2011; 15(3):449–55.
[38] Dua S, Acharya UR, Chowriappa P, Sree SV. Wavelet based energy features for glaucomatous image classification. IEEE Trans Inf Technol Biomed 2012;16(1):80–7.
[39] Mookiah MRK, Acharya UR, Lim CM, Petznick A, Suri JS. Data mining technique for automated diagnosis of glaucoma using higher order spectra and wavelet energy features. Knowl Based Syst 2012;33:73–82.
[40] Kim PY, Iftekharuddin KM, Gunvant P, Tóth M, Garas A, Holló G, Essock EA. Feature-based glaucomatous progression prediction using scanning laser polarimetry (SLP) data. Proc SPIE 2011;7963:79633T.
[41] Noronha KP, Acharya UR, Nayak KP, Martis RJ, Bhandary SV. Automated classification of glaucoma stages using higher order cumulant features. Biomed Sig Process Control 2014;10:174–83.
[42] Yousefi S, Goldbaum MH, Balasubramanian M, Jung TP, Weinreb RN, Medeiros FA, Zangwill LM, Liebmann JM, Girkin CA, Bowd C. Glaucoma progression detection using structural retinal nerve fiber layer measurements and functional visual field points. IEEE Trans Biomed Eng 2014;61(4):1143–54.
[43] Ceccon S, Garway-Heath DF, Crabb DP, Tucker A. Exploring early glaucoma and the visual field test: classification and clustering using Bayesian networks. IEEE J Biomed Health Inf 2014;18(3):1008–14.
[44] Maheshwari S, Pachori RB, Acharya UR. Automated diagnosis of glaucoma using empirical wavelet transform and correntropy features extracted from fundus images. IEEE J Biomed Health Inf 2017;21(3):803–13.
[45] Maheshwari S, Pachori RB, Kanhangad V, Bhandary SV, Acharya UR. Iterative variational mode decomposition based automated detection of glaucoma using fundus images. Comput Biol Med 2017;88:142–9.
[46] Acharya UR, Bhat S, Koh JEW, Bhandary SV, Adeli H. A novel algorithm to detect glaucoma risk using texton and local configuration pattern features extracted from fundus images. Comput Biol Med 2017;88:72–83.
[47] Glaucoma public database http://medimrg.webs.ull.es/ [date of access: 15.07.17].
[48] Giancardo L, Meriaudeau F, Karnowski TP, Li Y, Garg S, Tobin Jr KW, Chaum E. Exudate-based diabetic macular edema detection in fundus images using publicly available datasets. Med Image Anal 2012;16:216–26.
[49] Magli E, Olmo G, Presti LL. Pattern recognition by means of the Radon transform and continuous wavelet transform. J Signal Process 1999;73:277–89.
[50] Jafari-Khouzani K, Soltanian-Zadeh H. Rotation-invariant multiresolution texture analysis using radon and wavelet transforms. IEEE Trans Image Process 2005;14:783–95.
[51] Zabih R, Woodfill J. Non-parametric local transforms for computing visual correspondence. European Conference on Computer Vision, 2; 1994. pp. 151–8.
[52] Kublbeck C, Ernst A. Face detection and tracking in video sequences using the modified census transformation. Image Vis Comput 2006;24(6):564–72.
[53] Oliva A, Torralba A. Modeling the shape of the scene: a holistic representation of the spatial envelope. Int J Comput Vis 2001;42(3):145–75.
[54] GIST descriptors. Information available at: http://www.quora.com/Computer-Vision/What-is-a-GIST-descriptor# [date accessed on 04.07.17].
[55] Acharya UR, Fujita H, Bhat S, Raghavendra U, Gudigar A, Molinari F, Vijayananthan A, Ng KH. Decision support system for fatty liver disease using GIST descriptors extracted from ultrasound images. Inf Fus 2016;29:32–9.
[56] Raghavendra U, Acharya UR, Gudigar A, Tan JH, Fujita H, Hagiwara Y, Molinari F, Kongmebhol P, Ng KH. Fusion of spatial gray level dependency and fractal texture features for the characterization of thyroid lesions. Ultrasonics 2017;77:110–20.
[57] Acharya UR, Raghavendra U, Fujita H, Hagiwara Y, Koh JEW, Tan JH, Sudarshan VK, Vijayananthan A, Yeong CH, Gudigar A, Ng KH. Automated characterization of fatty liver disease and cirrhosis using curvelet transform and entropy features extracted from ultrasound images. Comput Biol Med 2016;(79):250–8.

[58] Raghavendra U, Acharya UR, Fujita H, Gudigar A, Chokkadi S. Application of Gabor wavelet and locality sensitive discriminant analysis for automated identification of breast cancer using digitized mammogram images. Appl Soft Comput 2016;46:151–61.
[59] Raghavendra U, Acharya UR, Ng EYK, Tan JH, Gudigar A. An integrated index for breast cancer identification using histogram of oriented gradient and kernel locality preserving projection features extracted from thermograms. Quant Infrared Thermogr J 2016;13(2): 195–209.
[60] Gudigar A, Chokkadi S, Raghavendra U, Acharya UR. Multiple thresholding and subspace based approach for detection and recognition of traffic sign. Multimed Tools Appl 2016;76(5):6973–91.
[61] Gudigar A, Chokkadi S, Raghavendra U, Acharya UR. An efficient traffic sign recognition based on graph embedding features. Neural Comput Appl 2017. http://dx.doi.org/10.1007/s00521-017-3063-z
[62] Gudigar A, Chokkadi S, Raghavendra U, Acharya UR. Local texture patterns for traffic sign recognition using higher order spectra. Pattern Recognit Lett 2017;94:202–10.
[63] Rao A, Noushath S. Survey: subspace methods for face recognition. Comput Sci Rev 2010;4(1):1–17.
[64] Cai D, He X, Zhou K, Han J, Bao H. Locality sensitive discriminant analysis. Proceedings of the 20th International Joint Conference Artificial Intelligence; 2007. p. 708–13.
[65] Saeys Y, Inza I, Larranaga P. A review of feature selection techniques in bioinformatics. Bioinf Rev 2007;23(19): 2507–2517.
[66] Obuchowski NA. Receiver operating characteristic curves and their use in radiology. Radiology 2003;229:3–8.
[67] T-test, Student's *t*-tests. Information available at: http://www.physics.csbsju.edu/stats/t-test.html [date accessed on 04.07.17].
[68] Dash M, Liu H. Handling large unsupervised data via dimensionality reduction. ACM SIGMOD Workshop on Research Issues in Data Mining and Knowledge Discovery; 1999.
[69] Abe N, Kudo M. Entropy criterion for classifier-independent feature selection. Knowledge-based intelligent information and engineering systems. Lect Notes Comput Sci 2005;3684:689–95.
[70] Lopes N. Comparing machine learning algorithms with the Wilcoxon Signed Rank Test. Information available at: http://www.uc.pt/fctuc/dei/statisticalHypothesis/noel [date accessed on 04.07.17].
[71] Hwang T, Sun CH, Yun T, Yi GS. FiGS: a filter-based gene selection workbench for microarray data. BMC Bioinf 2010;11. Information available at: http://www.biomedcentral.com/1471-2105/11/50 (date accessed on 04.07.17)..
[72] Natarajan S, Lipsitz SR, Fitzmaurice GM, Sinha D, Ibrahim JG, Haas J, Gellad W. An extension of the Wilcoxon Rank-Sum test for complex sample survey data. Journal of the Royal Statistical Society Series C Applied Statistics 2012; 61(4):653–64.
[73] Yuan Y, van Allen EM, Omberg L, Wagle N, Amin-Mansour A, et al. Assessing the clinical utility of cancer genomic and proteomic data across tumor types. Nat Biotechnol 2014;32:644–52.
[74] Kailath T. The divergence and Bhattacharyya distance measures in signal selection. IEEE Trans Commun Technol 1967;15(1):52–60.
[75] Vapnik V. The nature of statistical learning theory. New York: Springer-Verlag; 1995.
[76] Burgess CJC. A tutorial on support vector machines for pattern recognition. Data Min Knowl Discov 1998;2(2):1–47.
[77] Osareh A, Mirmehdi M, Thomas B, Markham R. Comparison of colour spaces for optic disc localization in retinal images. Proc. 16th Int. Conf. Pattern Recog., 1. 2002. pp. 743–6.
[78] Lowell J, Hunter A, Steel D, Basu A, Ryder R, Fletcher E, Kennedy L. Optic nerve head segmentation. IEEE Trans Med Imaging 2004;23(2):256–64.
[79] Townsend KA, Wollstein G, Danks D, Sung KR, Ishikawa H, Kagemann L, Gabriele ML, Schuman JS. Heidelberg Retina Tomograph 3 machine learning classifiers for glaucoma detection. Br J Ophthalmol 2008;92:814–8.
[80] Fink F, Worle K, Gruber P, Tome AM, Gorriz-Saez JM, Puntonet CG, Lang EW. ICA analysis of retina images for glaucoma classification. Engineering in Medicine and Biology Society, EMBS 2008, 30th Annual International Conference of the IEEE. 2008. pp. 4664–7.
[81] Nagarajan R, Balachandran C, Gunaratnam D, Klistorner A, Graham S. Neural network model for early detection of glaucoma using multi-focal visual evoked potential (M-Vep). Invest Ophthalmol Vis Sci 2002;42.
[82] Bock R, Meier J, Nyúl LG, Hornegger J, Michelson G. Glaucoma risk index: automated glaucoma detection from color fundus images. Med Image Anal 2010;14:471–81.
[83] Huang ML, Chen HY, Huang WC, Tsai YY. Linear discriminant analysis and artificial neural network for glaucoma diagnosis using scanning laser polarimetry – variable cornea compensation measurements in Taiwan Chinese population. Graefe's Arch Clin Exp Ophthalmol 2010;248(3):435–41.
[84] Kolar R, Jan J. Detection of glaucomatous eye via color fundus images using fractal dimensions. Radio Eng 2008; 17(3):109–14.
[85] Acharya UR, Ng EYK, Eugene LWJ, Noronha KP, Min LC, Nayak KP, Bhandary SV. Decision support system for the glaucoma using Gabor transformation. Biomed Signal Process Control 2015;15:18–26.
[86] Larose DT. Discovering knowledge in data: an introduction to data mining. New Jersey, USA: Wiley Interscience; 2004.
[87] Rodríguez AEG, Trinidad JFM, Borroto MG, Ochoa JAC. Mining patterns for clustering on numerical datasets using unsupervised decision trees. Knowl Syst 2015;82:70–9.
[88] Huang ZH, Li WJ, Wang J, Zhang T. Face recognition based on pixel-level and feature-level fusion of the top-level's wavelet sub-bands. Inf Fus 2015;22:95–104.
[89] Khan A, Farooq H. Principal component analysis-linear discriminant analysis feature extractor for pattern recognition. IJCSI Int J Comput Sci Issues 2011;8(6):267–70.
[90] Scikit Learn, LDA and QDA. Information available at: http://scikit-learn.org/stable/modules/lda qda.html [last accessed in November 2017].
[91] Sugeno M. Industrial applications of fuzzy control. Elsevier Science Pub. Co.; 1985.